This is a peer-reviewed, accepted author manuscript of the following article: Korobeinyk, A. V., Whitby, R. D. L., Mikhalovsky, S. V., & Inglezakis, V. J. (2019). In situ production of high purity noble metal nanoparticles on fumed silica and catalytic activity towards 2-nitrophenol reduction. *Journal of Physics and Chemistry of Solids* , *127*, 28-34.
https://doi.org/10.1016/j.jpcs.2018.12.001

In situ production of high purity noble metal nanoparticles on fumed silica and catalytic activity towards 2-nitrophenol reduction

Alina V. Korobeinyk[1,2,3], Raymond D.L. Whitby[2], Sergey V. Mikhalovsky,[4,5] and Vassilis J. Inglezakis[1,2]*

[1] The Environment & Resource Efficiency Cluster (EREC), Nazarbayev University, Astana, Kazakhstan
[2]Environmental Science & Technology Group (ESTg), Chemical Engineering Department, School of Engineering, Nazarbayev University, Astana, Kazakhstan
[3] O.O. Chuiko Institute of Surface Chemistry of NAS of Ukraine, Kyiv, Ukraine
[4] ANAMAD Ltd, Sussex Innovation Centre, Falmer, Brighton, UK
[5]SD Asfendiyarov KazakhNational Medical University, Almaty, Kazakhstan

**vasileios.inglezakis@nu.edu.kz*

Abstract

In-situ synthesis of chemically pure noble metal (Au, Pt, Pd, Ru) nanoparticles was performed via redox reaction under ambient conditions from aqueous noble metal salt solutions on non-porous fumed silica. Nanoparticles of average sizes < 5 and up to 19 nm were obtained. The nanostructured fumed silica with surface modified by triethoxysilane has been proven an effective support for noble metal nanoparticles synthesis. The silicon-hydride groups on the silica surface not only directly reduce noble metal ions from solution, but they also stabilize metal nanoparticles by bonding with the solid matrix. The nanocomposites were studied for the reduction of 2-nitrophenol showing very high activity at room temperature following the order Pd>Au>Ru>Pt.

Keywords: *fumed silica, noble metal, nanoparticles, redox, silicon-hydride, 2-nitrophenol*

Highlights

- Novel Au, Pt, Pd and Ru/silica nanocomposites were obtained via redox reaction over siliconhydride groups;
- Synthesised nanocomposites were characterised and tested in reaction of catalytic hydrogenation of 2-nitrophenol;
- Despite its similar molar loading Pd/SiO_2 has demonstrated a higher activity in catalytic reaction than the others;
- The pseudo-first-order rate constants of 2-nitrophenol hydrogenation calculated for Pt, Ru and Au nanocomposites were $1.3 \cdot 10^{-1}$ min^{-1}, $8.2 \cdot 10^{-1}$ min^{-1} and $8.6 \cdot 10^{-1}$ min^{-1}.

1. Introduction

Nitrophenols are among the most hazardous organic pollutants released from the production of pesticides, pharmaceuticals, plastics, explosives, solvents and dyes. Besides toxicity, nitrophenols are soluble and difficult to remove from wastewater by conventional wastewater treatment processes [1]. A promising method is the catalytic reduction of nitrophenols, a rapid reaction producing aminophenols. The catalytic reduction using sodium borohydride as reductant and noble metal nanoparticles as catalyst has been demonstrated to be an effective combination and the reaction has been used as a model for the study of

catalytic activity of nanoparticles (NPs) in aqueous solution [2-5]. 4-nitrophenol is by far the most studied nitrophenol and several noble NPs support materials have been used such as carbons, polymers, metal- and covalent-organic frameworks, oxides and porous silica. 2-nitrophenol (2-NPh) studies are less; Pd NPs on chitosan and metal-organic frameworks, core-shell Ag@Pt nanoparticles supported on sepiolite nanofibers, Ag-deposited silanized magnetite and Au–Pd bimetallic foams have been reported catalysts in reaction of 2-NPh reduction [5-9].

The remarkable reactivity of nanoparticles of Pt-group metal makes them excellent catalysts for chemical reactions, but in dispersion individual nanoparticles have tendency to agglomerate [10]. Another challenge is the non-uniformity of the NPs size [11]. A way to prevent undesirable aggregation and obtain uniform NPs size is the anchoring of metals on the surface of suitable support materials but the support materials may impede the activity of the NPs [3]. Thus, when synthesising NPs-containing nanocomposites both the redox active agents and the support material must be carefully selected. Various [12-15] support media were successfully utilized for metal NP anchoring via chemical [16] and physical [17, 18] methods. Non-porous and mesoporous silica were recently successfully utilised in the anchoring of several noble NPs, such as Ag, Pt, Pd and Au [11, 19-21]. An alternative support is fumed silica, an amorphous non-porous silicon dioxide composed of primary particles of around 1–3 nm which is fused to produce stable aggregates of around 50 nm. Owing to the large specific surface area of the formed agglomerates in the range of 300–350 m^2/g and thermal stability, fumed silica is an attractive material for utilization as NPs support and has been used for the synthesis of Ag NPs [22].

A problem with conventional synthesis methods is the use of chemical or other reducing agents and stabilizers, which result in impurities on the surface of the NPs. Silicon hydride compounds have long been used as reducing agents [23]. Modification of the silica surface with redox active chemical groups such as silicon-hydride may provide a suitable reaction platform for generating NPs with their simultaneous immobilization and stabilization on the surface of the matrix avoiding the use of other reducing reagents. This approach has been followed for the anchoring of Ag, Au, Pt and Pd on mesoporous silica (MCM-41 and Silochrom) [11, 20, 24, 25], Ag on fumed silica (surface area of 114m^2/g) and Au and Pd on pyrogenic silica (Aerosil, surface area of 120 m^2/g) [26-28].

In the present work, further investigation of the Si-H group reactivity in synthesis of noble metal (Au, Pt, Pd and Ru) SiO_2 composites by using a high surface area fumed silica (395 m^2/g) is reported. The ligand-free metal nanoparticles are stabilized on the SiO_2 matrix via bonding between the outer atoms of the nanoparticle and the silica surface. Extension of the silicon-hydride group reactivity to formation of metal nanoparticles for Pt and Ru is opening a one-step pathway for synthesis of pure NPs platinoid catalysts, electrodes and other useful materials. Furthermore, the catalytic hydrogenation of 2-nitrophenol with noble NPs was studied in order to demonstrate the catalytic properties of the synthesised nanocomposites.

2. Materials and Methods

2.1. Chemicals

$HAuCl_4.xH_2O$ (99.999% trace metals basis), H_2PtCl_6 (8 wt. % in H_2O), $Pd(NO_3)_2{\cdot}H_2O$ (~40% Pd basis), $RuCl_3{\cdot}H_2O$ (ruthenium content ~40%), $NaBH_4$ (99+%), 2-nitrophenol (99+%), SiO_2 (395 m^2/g), triethoxysilane (TEOS, 95%), acetic acid (glacial), acetone and ethanol (all from Sigma-Aldrich) were used as received. Ultrapure water (18.3 MΩ·cm) was used for all solutions.

2.2. Noble metal nanoparticle synthesis

The noble metal NPs/SiO_2 nanocomposites were prepared by *in-situ* redox reaction method. Silica surface was modified with TEOS in glacial acetic acid as described elsewhere [27, 28]. A mass of 1.0 g of TEOS-modified SiO_2 sample was immersed in 10 mM aqueous solutions of chloroauric acid ($HAuCl_4$), platinum hexachloride hydrate (H_2PtCl_6), palladium nitrate ($Pd(NO_3)_2$), and ruthenium chloride ($RuCl_3$) in order to create noble metal NPs loading of 0.2 mmol/g of silica. The mixture was stirred in the dark for 1 h to the

reaction completion, i.e. until all metal ions are removed from the liquid phase. Considering discoloration of Au, Pt, Pd and Ru salt solution during the NP formation over the silica surface a reaction completion was monitored by UV-Vis absorption spectroscopy. The qualitative comparison of the UV-Vis spectra shows excellent correlation between the times of contact of a chloroauric acid with silicon-hydride modified silica and reduction in the peak intensities determined via UV-Vis at 308 nm. As for the platinoids such correlation was determined at 260 (H_2PtCl_6, [29]), 465 ($Pd(NO_3)_2$, [30]), and 402 nm ($RuCl_3$, [31]), respectively. The mixture was then filtered and dried in a bench oven at 105 °C for 8 h.

2.3. Characterization of materials

FTIR spectra were recorded on a Nicolet Nexus 470 spectrometer in 4000-400 cm^{-1} range in order to identify a silica surface functionality. Transmission electron microscopy (TEM) analysis was carried out using a JEOL-JEM2100 instrument operated at 200 keV. High resolution TEM (HRTEM) images were captured using a Titan G2 60–300 transmission electron microscopy. Wide-angle X-ray diffraction (XRD) measurements were made on a Rigaku SmartLab diffractometer equipped with a CuKα radiation source (0.1549 nm) over the 2θ range from 10° to 90°. The mean crystalline size of the nanoparticles was calculated by the Scherrer's equation using the XRD data. Also, TEM images were used for the mean particle size determination where appropriate. The surface area was measured using the Brunauer, Emmet, and Teller (BET) method on an AutoSorb iQ (Quantachrome Instruments) following degassing at 150 °C. Noble metal ions concentrations were determined using a WTW photoLab 6600 UV-Vis (SpectroFlex 6600).

2.4 Catalytic reduction of 2-nitrophenol

Catalytic hydrogenation of 2-NPh in water was performed as follows: in the standard quartz cuvette with a 10 mm path length, 5 mg of nanocomposite was dispersed in 1.5 cm^3 of 1 mmol 2-NPh. Then, addition of 1.5 cm^3 of aqueous 0.01 mol dm^{-3} sodium borohyride to the reaction mixtures caused the decrease in the intensity of the peak of 2-NPh. The absorption spectra were recorded with UV−visible spectrophotometer (WTW photoLab 6600 UV-Vi) every 1 min in the range of 190−800 nm at 20 °C. The products of catalytic reduction of 2-NPh were identified by gas chromatography (GC-MS-MS, Thermo Scientific TSQ 8000 Evo). Sample preparation was made using 10 ml of sample and Bond Elut Plexa cartridge in methanol.

3. Results and discussion

3.1 Formation of noble metal nanoparticles on the silica surface

Non-porous silica modified with TEOS as described above is composed of uniform nanoparticles of 30-50 nm [32]. These particles contained Si-H surface groups which reduced noble metal ions in aqueous solutions. FTIR analysis (Fig.1) confirms the formation of silicon-hydride groups on the silica surface by the presence of adsorption band at 2240 cm^{-1} [33], which disappears after reaction with noble metal salt solution. The broad absorption band at 3300–3800 cm^{-1} is attributed to the adsorbed water and perturbed ≡SiOH groups in the surface layer while the band at 3750 cm^{-1} corresponds to O–H stretching vibrations of free surface silanol groups is absent [33]. The concentration of the Si-H groups on the silica surface was determined via iodometric titration [34] as 0.8 mmol/g. Reaction of Si-H modified silica surface with noble metal ions occurs with hydrogen gas formation (bubbling), indicating a redox pathway [11]. Although the only possible gas liberated is hydrogen, the insignificant amount of gas formed makes it impossible to capture and analyze it.

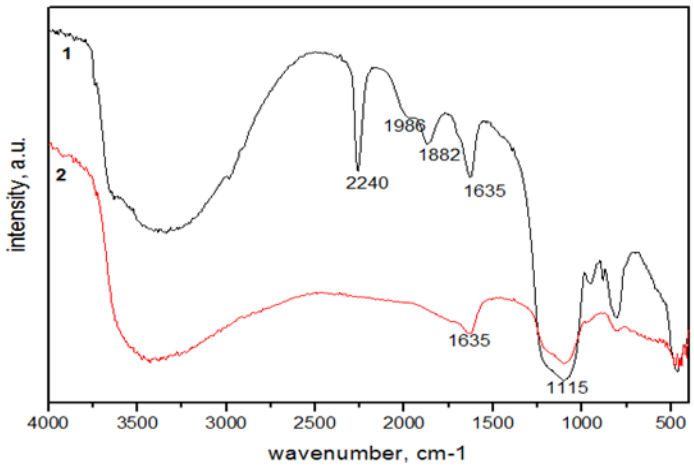

Fig.1. FTIR spectra of TEOS-modified SiO_2 (a) and Au NP/SiO_2 (b) samples.

Fig. 2 shows UV-visible spectra of chloroauric acid and platinum hexachloride hydrate recorded in respect to the times of contact with silicon-hydride modified silica. Over the time of reaction with the surface of silica, narrow symmetrical absorption band at 308 nm of the chloroauric acid solution disappears. This is attributed to metal ions conversion to metallic nanoparticles. No absorption was observed at wavelength longer than 350 nm (Fig. 2a). This implies that all gold nanoparticles are formed at the support media surface. In spectra of platinum hexachloride hydrate after contact with redox active surface band of H_2PtCl_6 disappears after 30 min of contact time (Fig. 2b). Same pattern were observed in UV-vis spectra of palladium nitrate and ruthenium chloride solutions (not shown here).

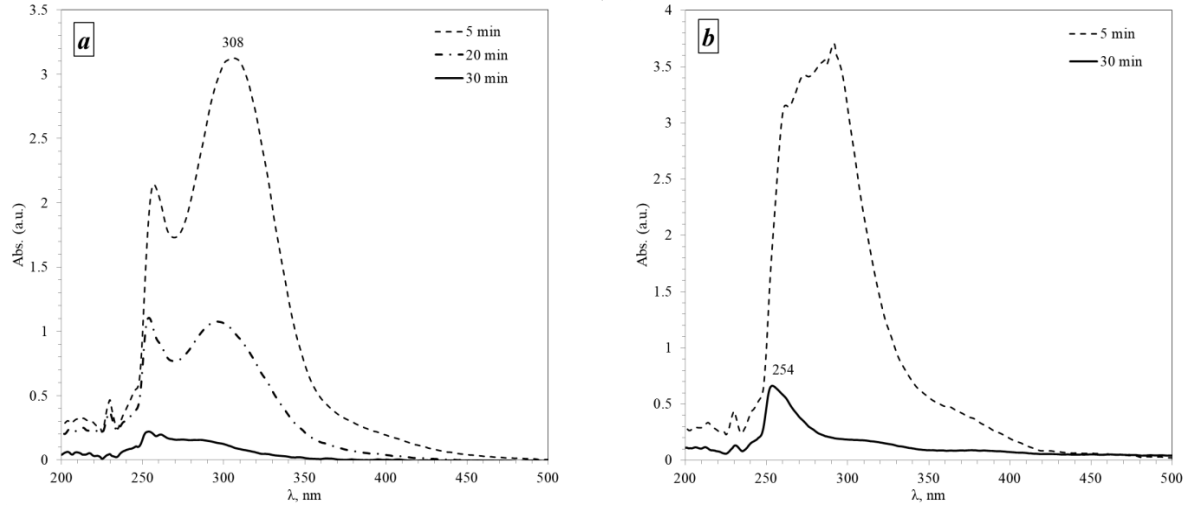

Fig. 2. UV-Vis spectra of chloroauric acid (a) and platinum hexachloride hydrate (b) solutions recorded versus contact time .

After reduction the original white silica (Fig. 3a), changed its colour to a red-brick colour with Au (Fig. 3b), and a light brown (Fig. 3c), beige (Fig. 3d) and black (Fig. 3e) colours were obtained for Pt, Pd and Ru, respectively. Apparently, these colours are related to the plasmon absorption of the corresponding metal nanoparticles [35-37]. These data are in agreement with the data obtained for non-immobilized nanopartlces of Au, Pt, Pd, and Ru, respectively, and support the formation of their respective NPs on the silica surface.

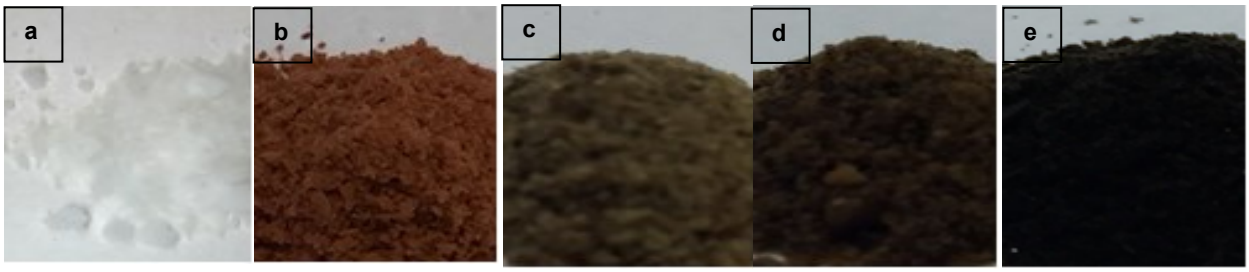

Fig. 3. Photos of Silica samples with (a) none, (b) Au, (c) Pt, (d) Pd, and Ru (e) metallic nanoparticles at 0.2 mmol/g metal loading.

The formation of metal nanoparticles was confirmed by TEM observations. Fig. 4 and 5 show TEM images and EDX spectra of metal nanoparticles on the SiO_2 surface. The presence of Au (Fig. 4a), Pt (Fig. 4b), Pd (Fig. 4c) and Ru (Fig. 4d) nanoparticles is evident. The largest particles are Au NPs, with mean diameter of 19 nm (Fig. 4a). The particle size of NPs was estimated to be 5.4 nm for Pt, 3.2 nm for Pd and 4.2 nm for Ru (**Error! Reference source not found.**b), respectively. The particle size of Au and Pd NPS are close to those reported elsewhere for pyogenic silica [11, 26]. At large magnification the crystalline lines within the nanoparticle structure of noble metal NPs are clearly seen (Fig. 6a). The metal/silica ratio and the size distribution of the metal nanoparticles obtained were compared at the same concentration of metal ion for all noble metal salts. The results showed similarity in noble NPs diameters at the same metal/silica ratio, except for Au. This trend is in agreement with the TEM images shown in Fig. 4 and 6. Thus, the loading of metal ion in contact with silica plays an important role in the NP size formation.

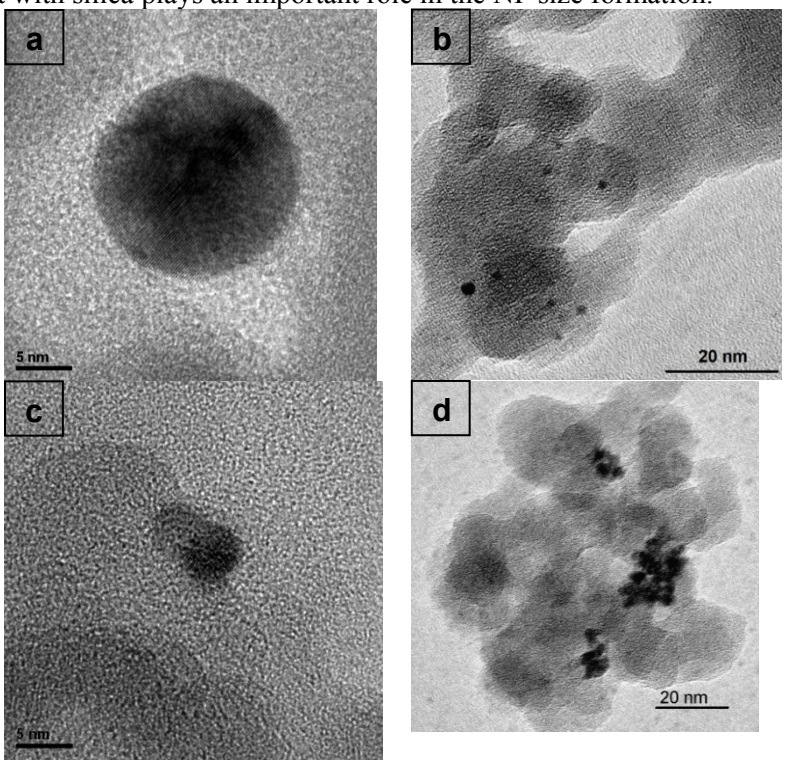

Fig. 4. High-resolution TEM images of as-prepared samples at 0.2 mmol/g metal loading of (a) Au/SiO_2, (b) Pt/SiO_2, (c) Pd/SiO_2, and (d) Ru/SiO2.

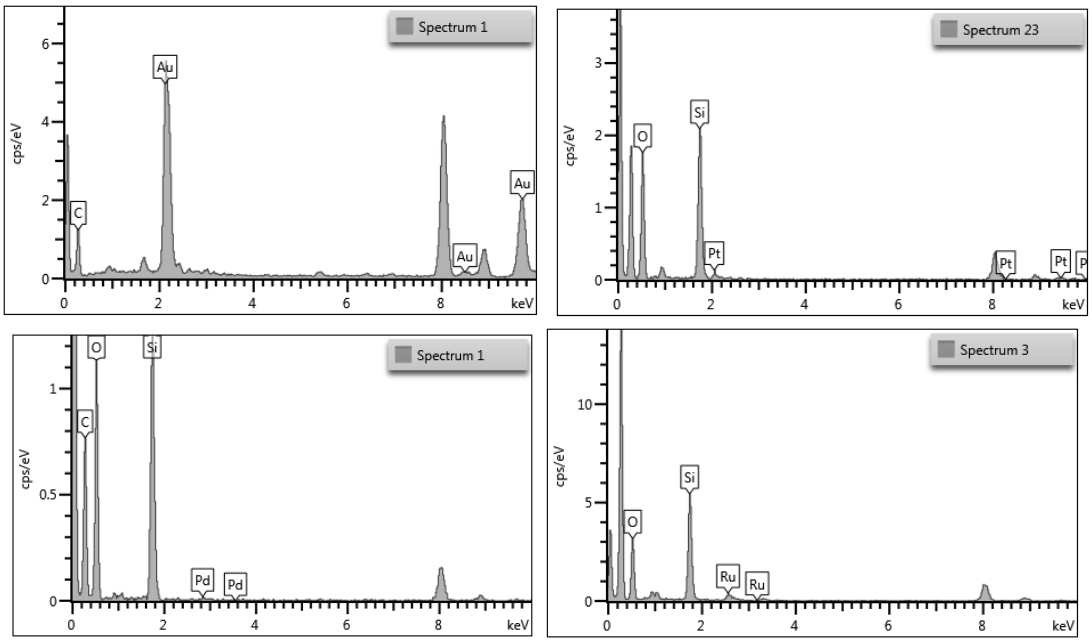

Fig. 5. TEM-EDX spectra of the nanocomposites.

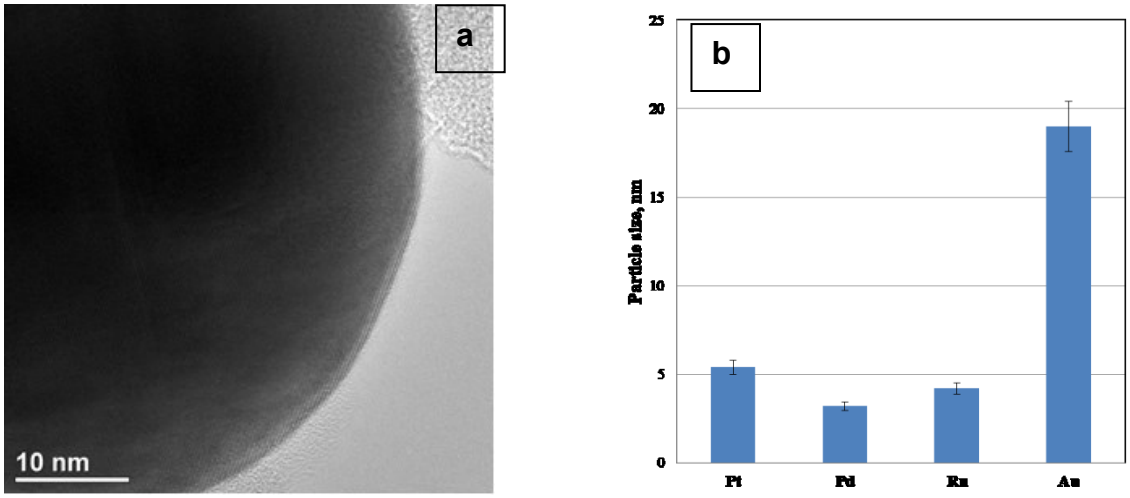

Fig. 6. (a) High-resolution TEM image of as-prepared Au/SiO_2 nanocomposites and (b) NPs average size at 0.2 mmol/g metal loading.

Nitrogen adsorption/desorption isotherms of all analysed samples belong to Type III (Fig. 7), characteristic for non-porous or macroporous materials. It was found that after modification with TEOS of the initial SiO_2 sample (395 m^2/g) the values of specific surface changes insignificantly (368.2 m^2/g), however surface areas of Au and Pd (186.2 and 124.8 m^2/g) is almost twice as smaller as that of Ru and Pt (354.6 and 356.8 m^2/g) modified samples. Generally, larger surface area in non-porous solids is associated with smaller particle sizes in a sample. Therefore reduction in specific surface area during the synthesis is related to the silica primary particles fusion, which reflected in values of the pore volume measured at saturation. The volume of N_2 adsorbed in TEOS modified silica sample was 2.79 $cm^3\ g^{-1}$, whereas the Pd loaded sample showed the lowest surface area and a adsorbed volume of of 1.19 $cm^3\ g^{-1}$; Au, Ru and Pt loaded samples shown values of 1.78, 1.52 and 1.49 $cm^3\ g^{-1}$, respectively.

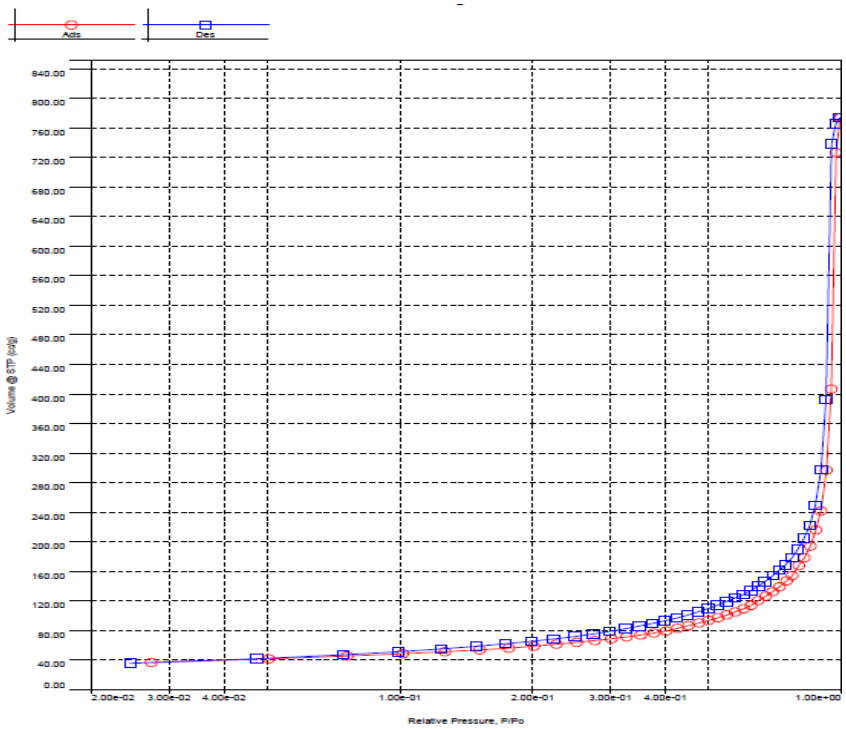

Fig. 7. BET adsorption-desorption isotherms of the Pd/SiO_2 sample.

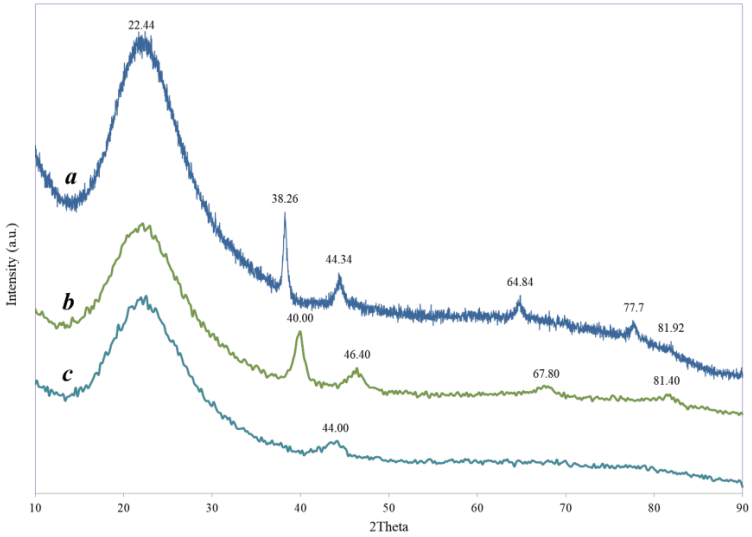

Fig. 8. XRD spectra of gold (a), platinum (b) and ruthenium (c) nanocomposites with 0.2 mmol/g metal loading.

XRD analysis of Au/SiO_2 NPs (Fig. 8a) revealed a clear pattern of five bands at 2θ values of 38.26°, 44.34°, 64.84°, 77.7° and 81.92° that correspond to (111), (200), (220), (311) and (222) planes of cubic Au(0) crystals, respectively. All the peaks in XRD pattern can be readily indexed to a structure of nanocrystalline gold [20]. Spectral bands of Pd(0) in XRD graph of the Pd/SiO_2 sample are not resolved (not shown here), this can be attributed to the formation literally monodisperse NPs distribution of very fine nanoparticles in the range of 5 nm (Fig. 4c). XRD pattern of Pt/SiO_2 (Fig.8b) was ascribed to cubic phase of Pt (0) and peaks at 40.00°, 46.40°, 67.80° and 81.40° were attributed to the main crystalline planes (111), (200), (220) and

(311). Formation of Ru/SiO_2 NPs clusters (Fig. 4c) correspond to the diffraction peak at 43.48° corresponding to (200) plane of cubic Ru(0) crystals (Fig. 8c) [11]. A large halo at 22.44° 2θ in all spectra emerges from the amorphous structure of silica support. No peaks of other crystalline phases have been detected.

3.2 Catalytic reduction of 2-nitrophenol

Upon the addition of sodium borohydride the two distinct absorption peaks of 2-NPh aqueous solution at 278 and 351 nm shift to 283 and 417 nm due to the formation of 2-nitrophenolate [6]. In absence of the catalytic nanocomposite a peak of 2-NPh at 417 nm remains unaltered. Fig. 9a shows representative UV-vis spectra of the reduction of 2-NPh by Pt/SiO_2 nanocomposite. The reduction can be visualised by the disappearance of the 417 nm peak in 15 min in presence of sodium borohydride and Pt/SiO_2 nanocomposite. The catalytic efficiency of Ru/SiO_2, Au/SiO_2 and Pd/SiO_2 nanocomposites was greater as compared to Pt/SiO_2 nanocomposite; the 417 nm peak disappear in 5 mins for Ru/SiO_2, 3 min for Au/SiO_2 and in case of Pd/SiO_2 discolouration take place at the time of sample addition. No adsorption band at 417 was registered in spectra of solution at zero time of reaction. For further comparison of the catalytic efficiency of metallic nanoparticles, the absorbance units change, expressed as $\ln(A_{417} - A_{550})$ as a function of reaction time was plotted (Fig. 9b) for samples loaded with different noble nanoparticles [6]. A linear correlation between $\ln(A_{417} - A_{550})$ and reaction time, indicates pseudo-first-order kinetic for sodium borohydride assisted reduction of the 2-NPh. The pseudo-first-order rate constant (k) for Pt/SiO_2, Ru/SiO_2 and Au/SiO_2 nanocomposites are 1.3×10^{-1} min^{-1}, 8.2×10^{-1} min^{-1} and 8.6×10^{-1} min^{-1}, respectively. Evidently, Pd/SiO_2 nanocomposite exhibits the highest catalytic efficiency.

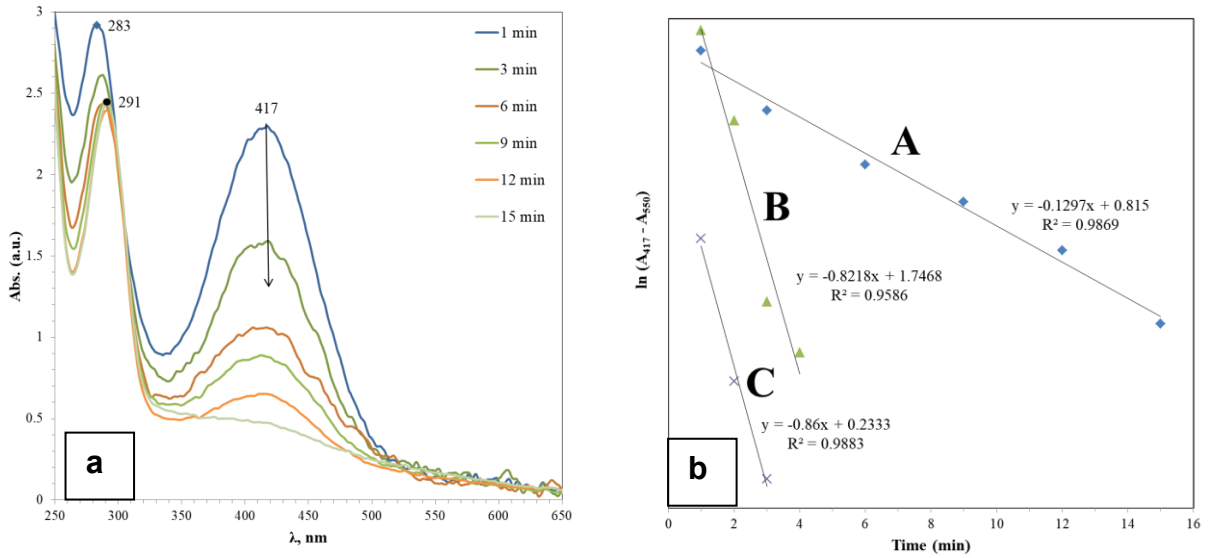

Fig. 9. UV-vis spectra of the reduction of 2-NPh by platinum (a) and (b) reaction kinetics analysis of 2-NPh reaction platinum (line A), ruthenium (line B) and Au (line C).

Direct hydrogenation of 2-NPh is practically impossible due to the high energy barrier between two negative ions [30]. Platinoid catalytic nanoparticles are particularly efficient in rapid generation of hydrogen from aqueous solutions of sodium borohydride [29]. Therefore the presence of catalytic nanoparticles is imperative for the reduction of 2-NPh. The proposed scheme (Fig. 10) explains the mechanism reaction as 2-NPh is diffuses form the aqueous solution to the catalytic NPs and then NPs are transferring the protons to 2-NPh molecule. The UV-vis peak shift from 283 nm to 291 nm can be attributed to the formation of 2-aminophenol [5]. Another peak shift observed in the literature is this of the 414 nm to 346 nm, indicating that $-NO_2$ is reduced to $-NH_2$ in the presence of Ag@Pt/sepiolite catalyst [1]. However,

this shift is not observed here or in other studies [6, 7]. The formation of 2-aminophenol was confirmed with GC-MS (Fig. 11).

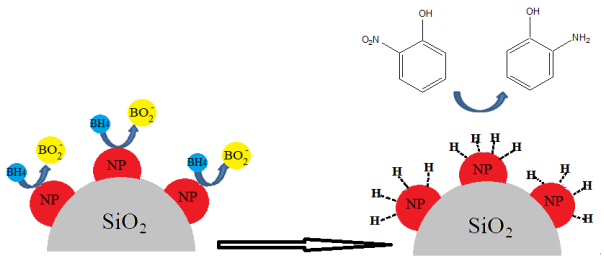

Fig. 10. A plausible mechanism for hydrogenation of 2-NPh by noble metal NPs/SiO_2 nanocomposites in the presence of borohydride ion.

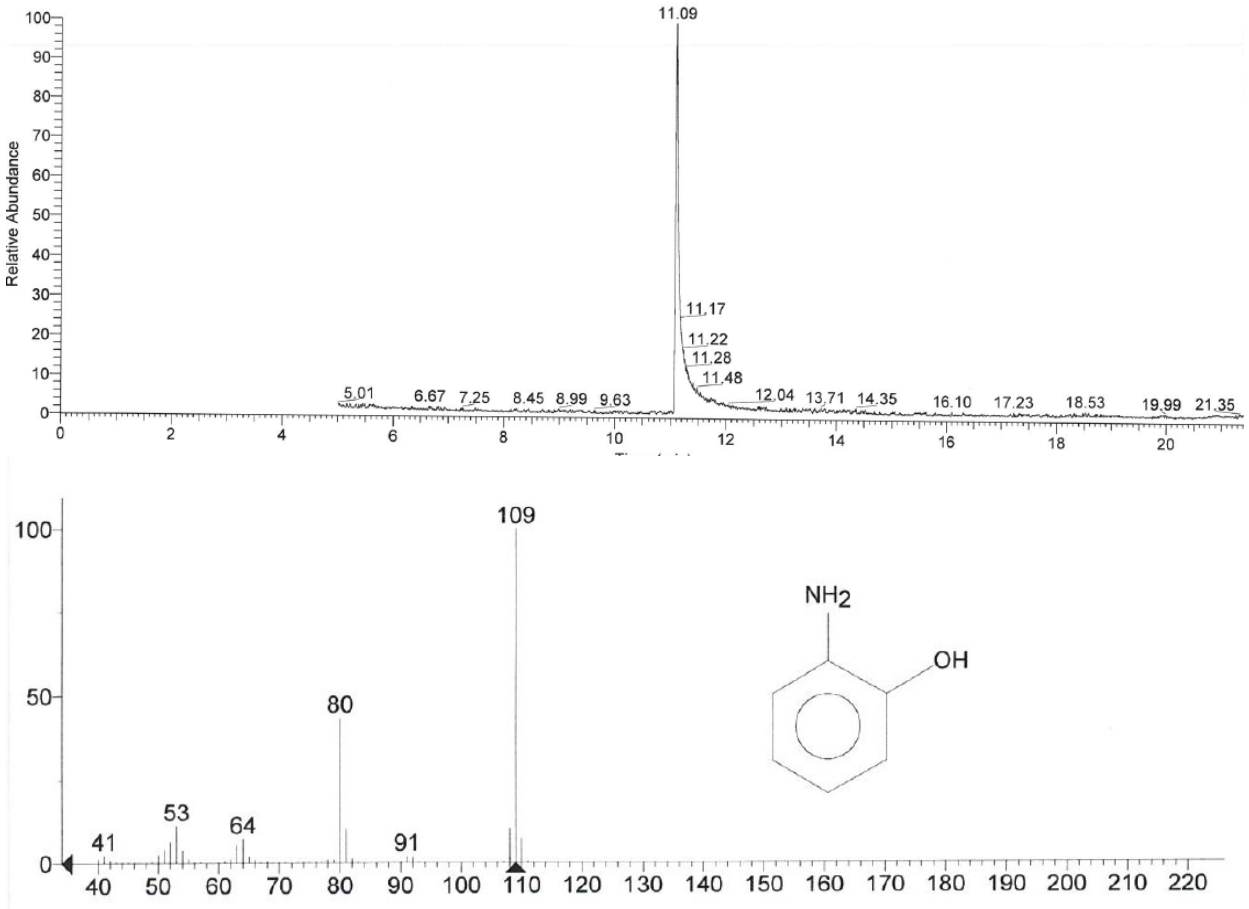

Fig.11. GC–MS chromatogram (top) and mass chromatogram (bottom) of the detected degradation product of 2-nitrophenol.

Conclusions

In this work we report a successful direct synthesis of a series of noble metal nanoparticles on non-porous silica surface modified with TEOS. This one-stage synthesis in aqueous environment and at ambient

temperature did not require the use of any reducing agents ensuring high purity of NPs. Under optimized conditions, monodisperse metal nanoparticles were obtained. The silica surface modified with redox-active silicon-hydride groups constitute an effective nanoreactor for in situ synthesis of metal nanoparticles in regards to heterogeneous nucleation and particle growth. Defect-free spherical nanoparticles obtained via reported method presumes layer by layer mechanism of crystal growth on the smooth surface of primary nucleus. The silicon-hydride groups not only reduce metal ions, but also stabilize metal nanoparticles by strong bonding on the silica surface. A practical application is implied to such materials as many practical uses of nanoparticles are possible only in solid supports. The in-situ synthetic approach is simple, cost-effective and environmentally friendly. It can provide a facile approach toward manufacturing of metallic nanocomposites, antimicrobial materials, low-temperature catalysts, and other useful materials. Among the four different metal nanocomposite tested, the Pd/SiO_2 nanocomposite showed the highest catalytic activity for the reduction of 2-NPh in aqueous solution at ambient temperature.

Acknowledgements

The authors express their gratitude to Dr Alex Jass, Serikbayev Ust' Kamenogorsk State University, Kazakhstan, for the TEM measurements and analysis. This work has been financially supported by Nazarbayev University project ORAU "HyperActiv" SOE 2015 009, the European Commission projectHorizon 2020 MSCA-RISE-2016 "NanoMed" and the Royal Academy of Engineering (UK) projects IAPP/1516/46 and IAPP/1516/3.

References

[1] Ma, Y., X. Wu, and G. Zhang, Core-shell Ag@Pt nanoparticles supported on sepiolite nanofibers for the catalytic reduction of nitrophenols in water: Enhanced catalytic performance and DFT study. Applied Catalysis B: Environmental, 2017. **205**: p. 262-270. doi: 10.1016/j.apcatb.2016.12.025.

[2] Pradhan, N., A. Pal, and T. Pal, Silver nanoparticle catalyzed reduction of aromatic nitro compounds. Colloids and Surfaces A: Physicochemical and Engineering Aspects, 2002. **196**(2): p. 247-257. doi: 10.1016/S0927-7757(01)01040-8.

[3] Gu, S., et al., Kinetic analysis of the catalytic reduction of 4-nitrophenol by metallic nanoparticles. The Journal of Physical Chemistry C, 2014. **118**(32): p. 18618-18625. doi: 10.1021/jp5060606.

[4] Zhao, P., et al., Basic concepts and recent advances in nitrophenol reduction by gold- and other transition metal nanoparticles. Coordination Chemistry Reviews, 2015. **287**: p. 114-136. doi: 10.1016/j.ccr.2015.01.002.

[5] Dhanavel S., et al., Synthesis of chitosan supported palladium nanoparticles and its catalytic activity towards 2-nitrophenol reduction. AIP Conference Proceedings, 2016. **1731**(1): p. 050092. doi: 10.1063/1.4947746.

[6] Liu, H. and Q. Yang, Facile fabrication of nanoporous Au–Pd bimetallic foams with high catalytic activity for 2-nitrophenol reduction and SERS property. Journal of Materials Chemistry, 2011. **21**(32): p. 11961-11967. doi: 10.1039/C1JM10109A.

[7] Shin, K.S., et al., Facile synthesis of silver-deposited silanized magnetite nanoparticles and their application for catalytic reduction of nitrophenols. Applied Catalysis A: General, 2012. **413-414**: p. 170-175. doi: 10.1016/j.apcata.2011.11.006.

[8] Ma, T., et al., A comparison reduction of 4-nitrophenol by gold nanospheres and gold nanostars. Catalysts, 2017. **7**(2): p. 38. doi: 10.3390/catal7020038.

[9] Xu, B., et al., Pd@MIL-100(Fe) composite nanoparticles as efficient catalyst for reduction of 2/3/4-nitrophenol: Synergistic effect between Pd and MIL-100(Fe). Microporous and Mesoporous Materials, 2018. **255**: p. 1-6. doi: 10.1016/j.micromeso.2017.07.008.

[10] Esumi, K., R. Isono, and T. Yoshimura, Preparation of PAMAM− and PPI−metal (Silver, Platinum, and Palladium) nanocomposites and their catalytic activities for reduction of 4-nitrophenol. Langmuir, 2004. **20**(1): p. 237-243. doi: 10.1021/la035440t.

[11] Ivashchenko, N., et al., Potentialities of silane-modified silicas to regulate palladium nanoparticles sizes. Journal of Thermal Analysis and Calorimetry, 2012. **108**(3): p. 1121-1127. doi: 10.1007/s10973-011-2067-7.

[12] He, J., T. Kunitake, and A. Nakao, Facile in situ synthesis of noble metal nanoparticles in porous cellulose fibers. Chemistry of Materials, 2003. **15**(23): p. 4401-4406. doi: 10.1021/cm034720r.
[13] Gholamali, H., et al., Synthesis of Ag and Au nanoparticles embedded in carbon film: Optical, crystalline and topography analysis. Results in Physics, 2017. doi: 10.1016/j.rinp.2017.12.033.
[14] Tran, Q.C., et al., Polyhedral gold nanocrystals/polyelectrolyte composite film: One-pot synthesis via interfacial liquid plasma polymerization. Composites Science and Technology, 2017. **153**(Supplement C): p. 198-208. doi: 10.1016/j.compscitech.2017.10.021.
[15] Zhang, C., et al., Electron contributions to the heat conduction across Au/graphene/Au interfaces. Carbon, 2017. **115**(Supplement C): p. 665-671. doi: 10.1016/j.carbon.2017.01.051.
[16] Selvan, S.T., et al., Sol−gel derived gold nanoclusters in silica glass possessing large optical nonlinearities. The Journal of Physical Chemistry B, 2002. **106**(39): p. 10157-10162. doi: 10.1021/jp020860x.
[17] Alexandrov, A., et al., UV-initiated growth of gold nanoparticles in PMMA matrix. Applied Surface Science, 2005. **248**(1): p. 181-184. doi: 10.1016/j.apsusc.2005.03.002.
[18] Majid Kazemian, A., et al., Formation of gold nanoparticles in polymethylmethacrylate by UV irradiation. Journal of Physics D: Applied Physics, 2007. **40**(12): p. 3771.
[19] Liu, C.-Y., J.-J. Huang, and C.-H. Lai, Resistive switching characteristics of a Pt nanoparticle-embedded SiO_2-based memory. Thin Solid Films, 2013. **529**(Supplement C): p. 107-110. doi: 10.1016/j.tsf.2012.03.108.
[20] Tertykh V. A., et al., Platinum nanoparticles on the surface of silica modified with silicon hydride groups. Materialwissenschaft und Werkstofftechnik, 2013. **44**(2- 3): p. 239-243. doi: 10.1002/mawe.201300115.
[21] Mota-Santiago, P., et al., Elongation of metallic nanoparticles at the interface of silicon dioxide and silicon nitride. Nuclear Instruments and Methods in Physics Research Section B: Beam Interactions with Materials and Atoms, 2017. **409**(Supplement C): p. 328-332. doi: 10.1016/j.nimb.2017.03.068.
[22] Plumeré, N. and B. Speiser, Redox-active silica nanoparticles: Part 2. Photochemical hydrosilylation on a hydride modified silica particle surface for the covalent immobilization of ferrocene. Electrochimica Acta, 2007. **53**(3): p. 1244-1251. doi: 10.1016/j.electacta.2007.01.020.
[23] Keinan, E., Silicon hydrides in organic synthesis. Pure and Applied Chemistry, 1989. **61**(10): p. 1737-1746. doi: 10.1351/pac198961101737.
[24] Zienkiewicz-Strzałka, M., et al., Silver nanoparticles deposited on pyrogenic silica solids: Preparation and textural properties. Adsorption Science & Technology, 2017. **35**(7-8): p. 714-720. doi: 10.1177/0263617417707599.
[25] Ivashchenko N.A., et al., Silica with grafted silicon hydride groups and its application for preparation of palladium nanoparticles. Int. J. of Nanoparticles, 2011. **4**(4): p. 350-358.
[26] Tertykh V.A., Katok K.V., and V.V. Yanishpolskii, The reduction of gold nanoparticles in the surface layer of modified silica. Russian Journal of Physical Chemistry A, 2008. **82**(9): p. 1438-1441. doi: 10.1134/S0036024408090045.
[27] Katok, K.V., et al., Hyperstoichiometric interaction between silver and mercury at the nanoscale. Angewandte Chemie International Edition, 2012. **51**(11): p. 2632-2635. doi: 10.1002/anie.201106776.
[28] A.V. Korobeinyk and V.J. Inglezakis, Silver nanoparticles synthesised within the silica matrix in hyperstoichiometrical of mercury from aqueous solutions IOP Conf. Ser. Earth Environ. Sci. , 2018. **182**. doi: 10.1088/1755-1315/182/1/012013.
[29] Brack, P., S.E. Dann, and K.G.U. Wijayantha, Heterogeneous and homogenous catalysts for hydrogen generation by hydrolysis of aqueous sodium borohydride (NaBH4) solutions. Energy Science & Engineering, 2015. **3**(3): p. 174-188. doi: 10.1002/ese3.67.
[30] Lin, F.-h. and R.-a. Doong, Bifunctional Au−Fe_3O_4 heterostructures for magnetically recyclable catalysis of nitrophenol reduction. The Journal of Physical Chemistry C, 2011. **115**(14): p. 6591-6598. doi: 10.1021/jp110956k.
[31] Özkar, S. and M. Zahmakıran, Hydrogen generation from hydrolysis of sodium borohydride using Ru(0) nanoclusters as catalyst. Journal of Alloys and Compounds, 2005. **404-406**: p. 728-731. doi: 10.1016/j.jallcom.2004.10.084.
[32] Boldridge, D., Morphological characterization of fumed silica aggregates. Aerosol Science and Technology, 2010. **44**(3): p. 182-186. doi: 10.1080/02786820903499462.
[33] Bellamy, A.L.J., The infra-red spectra of complex molecules. 3rd ed. The best collection of infrared group frequencies. Vol. 1. 1975, London: Chapman and Hall. 380.

[34] Crompton, T.R. and T.R. Crompton, CHAPTER 6 - Iodometric methods for the analysis of organoaluminium compounds, in *Analysis of Organoaluminium and Organozinc Compounds*. 1968, Pergamon. p. 252-264.
[35] Abreu, D.d.S., et al., Electrochemical, surface enhanced Raman scattering and surface plasmon resonance investigations on the coordination of cyanopyridine to ruthenium on surface. Electrochimica Acta, 2014. **122**: p. 204-209. doi: 10.1016/j.electacta.2013.10.132.
[36] Atyaoui, M., et al., Enhancement in photovoltaic properties of silicon solar cells by surface plasmon effect of palladium nanoparticles. Superlattices and Microstructures, 2016. **92**: p. 217-223. doi: 10.1016/j.spmi.2016.01.028.
[37] Hazra, A., et al., Gold-silver nanostructures: Plasmon-plasmon interaction. Vacuum, 2017. **146**: p. 437-443. doi: 10.1016/j.vacuum.2017.05.016.